Revisiting Hot-Wire Anemometry Close to Solid Walls

Y. Ikeya[1,2], R. Örlü[2], K. Fukagata[1] and P. H. Alfredsson[2]
[1] *Department of Mechanical Engineering, Keio University, Yokohama, Japan*
[2] *Linné FLOW Centre, KTH Mechanics, Stockholm, Sweden*

ramis@mech.kth.se

Abstract

The present paper deals with the erroneous velocity reading of hot-wire anemometry close to a solid wall caused by additional heat losses examined by means of experiment and numerical simulation. Measurements in both quiescent air and laminar/turbulent-boundary layer confirmed the influences of parameters such as wall conductivity, overheat ratio and probe dimensions on the output voltage (not just the mean value but also its fluctuations). The accompanying two-dimensional numerical simulation indicated its usefulness for qualitative discussion of the problem.

1 Introduction

Hot-wire anemometry (HWA) has been the most widely used laboratory method to measure local fluid velocities in experimental fluid mechanics, which enabled the study of turbulent fluctuations quantitatively. Furthermore, it was the only method capable of measuring high frequency and amplitude velocity fluctuations with a high spatial resolution and has been dominant in the experimental field until the development of laser-based techniques such as laser Doppler velocimetry (LDV) and particle image velocimetry (PIV). HWA is therefore prominently in use for acquiring data in wall-bounded turbulent flows.

However, a well-known major drawback in HWA is that a hot-wire probe calibrated in the wall-remote region registers a seemingly higher velocity in the near-wall region, known as the wall-proximity effect. Additional heat losses from the heated sensor to the cooler wall are erroneously read as an increase in velocity as the wire approaches the wall surface. The wall-proximity effect causes a problem especially when the friction velocity, *the* characteristic scale in wall-bounded turbulence, needs to be deduced from the velocity profile in the viscous sublayer (Örlü et al., 2010).

The aforementioned problem has been investigated in numerous studies in the literature, with many of them concerned with possible correction schemes for the mean velocity and its dependence on operational and geometrical parameters. Generally, it is widely agreed upon that the wall conductivity, overheat ratio, and sensor dimensions have an influence on the erroneous velocity reading, such that:

- Highly conductive materials register larger apparent velocity reading than poorly conductive materials do (see e.g. Polyakov & Shindin, 1978; Bhatia et al., 1982; Durst & Zanoun, 2002).
- Larger length-to-diameter ratio l/d of the wire results in a larger apparent velocity reading (see e.g. Krishnamoorthy et al., 1985; Chew et al., 1995).
- The larger the overheat ratio is, the larger the apparent velocity reading becomes (see e.g. Krishnamoorthy et al., 1985; Zanoun et al., 2009).

However, the detailed principle of the heat transfer for the hot-wire in the near-wall region including its interaction with the wall material is still not entirely understood. In addition, most of the previous studies, if not all, are concerned with errors in the mean velocity and there is little, if not no, knowledge of the measured turbulence quantities: turbulence intensity and higher-order moments. In light of the recent demands for increased accuracies in determining the friction velocity and/or absolute wall-position (Örlü et al., 2010), the interest in higher-order moments in the near-wall region (Örlü et al., 2016) as well as its wall-limiting quantities, e.g. the fluctuating wall-shear stress (Alfredsson et al, 1988; Örlü & Schlatter, 2011), there is a need to revisit the effect of hot-wire measurements close to solid walls.

The present investigation carries out a systematic parameter study on the misreading of hot-wire anemometry in the near-wall region so that further insight can be provided into this field, which will eventually help researchers to investigate this topic effectively in the future. In particular, measurements under no-flow and flow conditions, in a laminar and a turbulent boundary layer, have been performed by varying the wall material, overheat ratio, and probe dimensions. Furthermore, a numerical investigation is carried out to further study the heat conduction inside the wall material.

2 Experimental Part

2.1 Natural convection measurements

To study the effect of parameters in the absence of a cross flow, measurements in a specially designed enclosed box were performed. The schematic of the setup is illustrated in figure 1. A probe mounted on a metallic arm can be vertically traversed manually by means of a micrometer. The output voltage of the anemometer was acquired at thirtyfive heights up to a distance of $y = 2$ mm from the wall. Additionally, the voltage output at $y = 5$ mm was recorded as E_0, where the effect of the wall is considered to be negligible.

The effect of thermal conductivity of the wall was investigated by changing the wall material between aluminum, brass, steel, Plexiglas, and styrofoam. Besides the wall material, the wire length and resistance overheat ratio

$$a_R = \frac{R_w - R_0}{R_0}\,, \tag{1}$$

were also taken as parameters to see their influence on the voltage reading. Here, the subscript 0 denotes the cold state, i.e. reference state, and w denotes the heated state, i.e. when the wire is under operation.

2.2 Wind-tunnel experiment

HWA measurements were also carried out inside the *Minimum Turbulence Level* (MTL) closed-loop wind tunnel located at the Royal Institute of Technology (KTH) in Stockholm, which has a 7 m long test section and a cross-sectional area of 0.8×1.2 m^2.

A probe is mounted on a traversing system above a flat plate as shown in figure 2 and can be controlled from a computer. The flat plate has both aluminum and Plexiglas surfaces at different spanwise positions at the same streamwise location, which were used to investigate the effect of wall conductivity. Furthermore, both laminar and turbulent boundary layers developing on the plate with zero-pressure gradient were considered with momentum-loss thickness Reynolds numbers (Re_θ) of around 400 and 950, respectively. The sampling frequency in this measurement is 20000 Hz and the sampling time is 10 seconds.

Calibration of the probes was carried out in the free-stream and upstream of the flat plate, against a Prandtl tube which was also used to monitor the free-stream velocity in the tunnel. The free-stream velocity is controlled by a computer and the corresponding voltage output from the probe is recorded. The voltage without flow E_0 is also recorded and used for the calibration. In the present study, a 4th-order polynomial was used to relate the top-of-the-bridge voltage to the velocity (see e.g. George et al., 1989).

2.3 Experimental results

Results from the measurements on different wall materials in quiescent air are depicted in figure 3a) and show, as expected, the dependency of the wall conductivity on the hot-wire reading (platinum core wire with 2.5 μm diameter and 0.6 mm nominal length operated at an resistance overheat ratio $a_R = 0.8$). In accordance with Durst et al. (2002), large differences can be observed between poorly conducting walls (Plexiglas and styrofoam with heat conductivities of the order of 10^{-1} and 10^{-2} W/mK, respectively), while the results from highly conducting materials (such as aluminum, brass and steel, with heat conductivities of the order of 10^1–10^2 W/mK) do not vary between each other. The dependency on the overheat ratio for the same probe on the aluminum wall, shown in figure 3b), is also in accordance with the main body of previous studies (Durst & Zanoun, 2002).

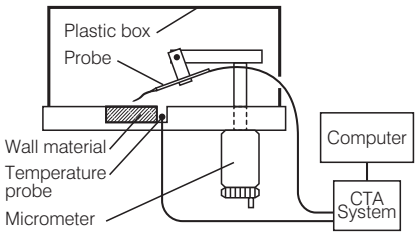

Figure 1: Schematic of the setup for the natural convection measurements.

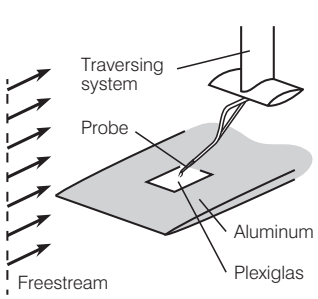

Figure 2: Schematic of the setup for the windtunnel experiments.

Figure 3c) shows the overheat ratio dependency in a laminar boundary layer, in which the overheat ratio exhibits the same effect as for the results in quiescent air; the higher the overheat ratio, the stronger the deviation from the linear profile. In both cases, the effect is however limited to $y^+ \lesssim 3$, where the superscript '+' denotes scaling in wall units.

The mean streamwise velocity and root-mean square profiles for a turbulent boundary layer are shown in figure 4a) for two different wall materials (aluminum and Plexiglass) and display no differences in the inner layer of the boundary layer. The marginal differences in the outer layer are due to slightly different conditions of the boundary layers (i.e. slight differences in the Reynolds number as well as probable inhomogeneities in the spanwise direction). One should, however, recall that the accurate determination of the absolute wall position in wall-bounded flows is by no means trivial (see Örlü et al., 2010), and that small difference can easily be "hidden" (due to inaccuracies in the absolute wall position and/or the determined friction velocity by shifting the profiles by less than one inner unit) in a semi-logarithmic plot. If one considers instead the profiles in the diagnostic plot (Alfredsson et al., 2011b) shown in figure 4b), which is independent of the wall position and the friction velocity, differences do appear in the region $U/U_\infty < 0.25$; which corresponds to the viscous sublayer (Alfredsson & Örlü, 2010). As apparent, the measured turbulence intensity (and in turn the related rms value of the fluctuating wall shear stress, i.e. $\tau_{w,\mathrm{rms}}/\tau_w = \lim_{y\to 0} u_{\mathrm{rms}}/U$) is reduced for highly conducting materials. To illuminate this effect further figure 4c) depicts the probability density distribution (PDF) for the streamwise velocity fluctuations in inner scaling. In accordance with Alfredsson et al. (2011a), the PDF contour lines should be parallel to each other in the viscous sublayer, which is observed for the contour lines at higher velocities. The deviation at lower velocities is more apparent for the highly conducting wall material. The aforementioned observations can also be made when considering the effect of the overheat ratio as demonstrated in figure 5.

3 Numerical Part

3.1 Physical model and boundary conditions

A two-dimensional numerical simulation using OpenFOAM (version 2.2.2) is conducted. In the present study, an infinitely long cylinder parallel to a wall and normal to the flow is employed to represent the hot-wire sensor as shown in figure 6. The entire computational domain is divided into a fluid and solid region.The wire centre is located at $(x/d,\ y/d) = (0,\ 100)$ and the domain spreads in the streamwise direction $-3000 < x/d < 6000$. The fluid region is from $0 < y/d < 5000$ and the solid region is from $-5000 < y/d < 0$. The mesh is created with ANSYS ICEM and the domain contains 339,040 points in its fluid region and 197,600 points in the solid region.

A Couette flow is reproduced to simulate the phenomenon of a hot wire located in the viscous sublayer.

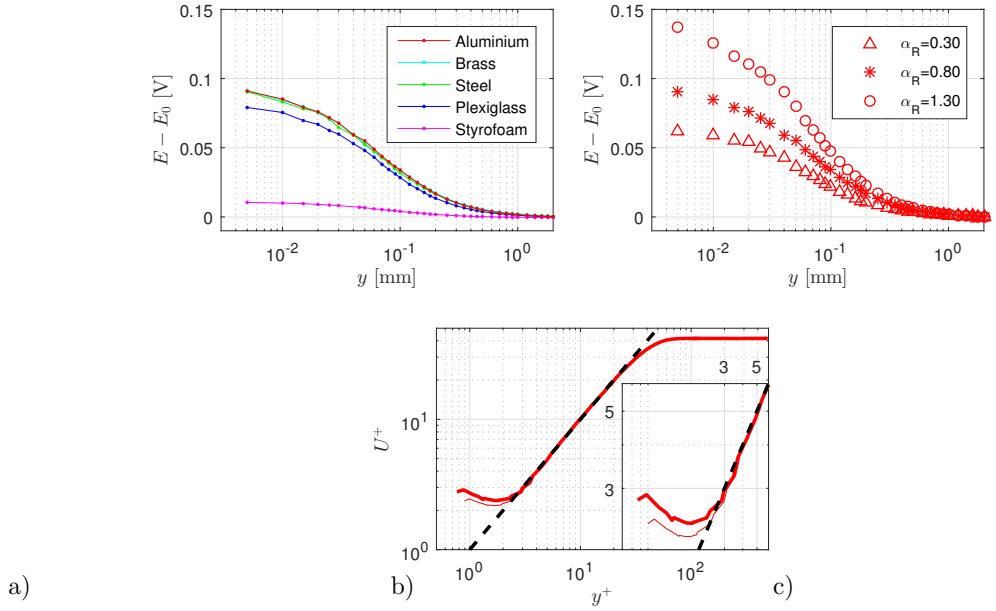

Figure 3: Voltage difference from hot-wire readings in quiescent air a) on different wall materials measured with a resistance overheat ratio $\alpha_R = 0.8$, and b) at different resistance overheat ratio measured on aluminum. c): Inner-scaled velocity profile in a laminar boundary layer at $Re_\theta \approx 400$ on the aluminum wall at a resistance overheat ratio of $a_R = 0.3$ (thin line) and $a_R = 0.8$ (thick line). Black dashed line indicates the linear profile $U^+ = y^+$.

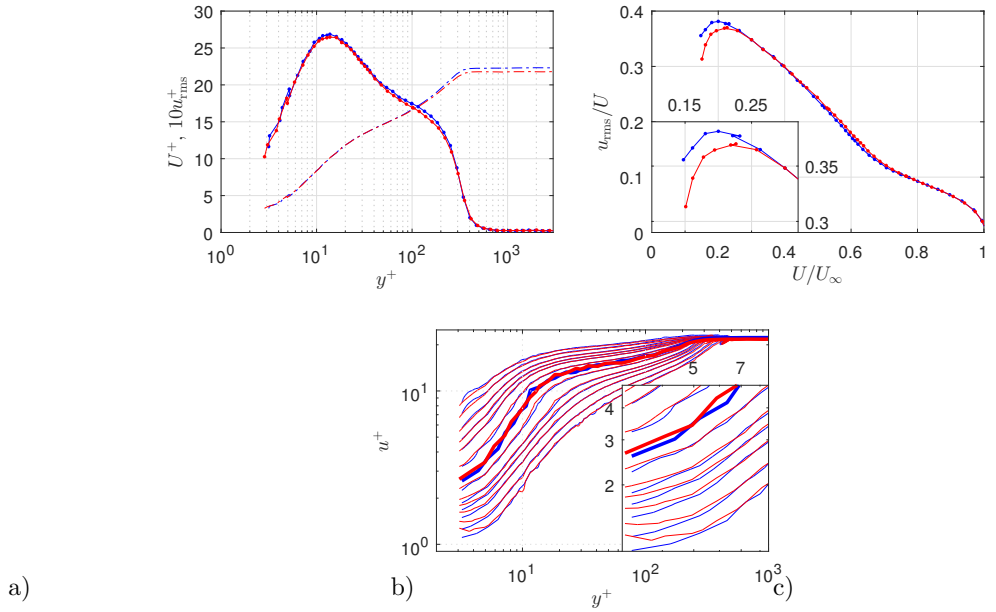

Figure 4: Effect of different wall materials in a turbulent boundary layer at $Re_\theta \approx 950$ measured with an resistance overheat ratio of $a_R = 0.8$: aluminum (red) and Plexiglass (blue). a): Inner-scaled mean and rms profile. b): Diagnostic plot with inset highlighting the viscous sublayer. c): Inner-scaled velocity PDF. Thin lines denote 1, 5, 20, 40, 60 and 90 % of the local maximum (thick line) of the PDF.

In the present calculation, the inner-scaled distance between the wire center and the wall surface is changed by varying the velocity gradient $S = dU/dy|_{\text{inlet}}$. The temperatures at the inflow and the top moving wall are set to $T_\infty = 20$ °C while the surface of the cylinder is set to $T_w = 100$ °C. No-slip conditions are applied at the solid walls and zero-gradient Neumann boundary conditions for velocity and temperature are applied at the outlet. In the solid region, the Dirichlet boundary condition $T = T_\infty$ was applied at the upstream wall, and adiabatic Neumann conditions were set at the bottom and the downstream boundaries. These two regions were coupled by means of the temperature continuity and heat flux conservation at the interfaces, namely,

$$T_{\text{fluid}} = T_{\text{solid}} \quad \text{and} \quad \left(k\frac{\partial T}{\partial y}\right)_{\text{fluid}} = \left(k\frac{\partial T}{\partial y}\right)_{\text{solid}}. \qquad (2)$$

The thermal conductivity of the solid region was set to $k_{\text{solid}} = 205$ and 0.19 W/(mK), corresponding to the properties of aluminum and Plexiglas, respectively.

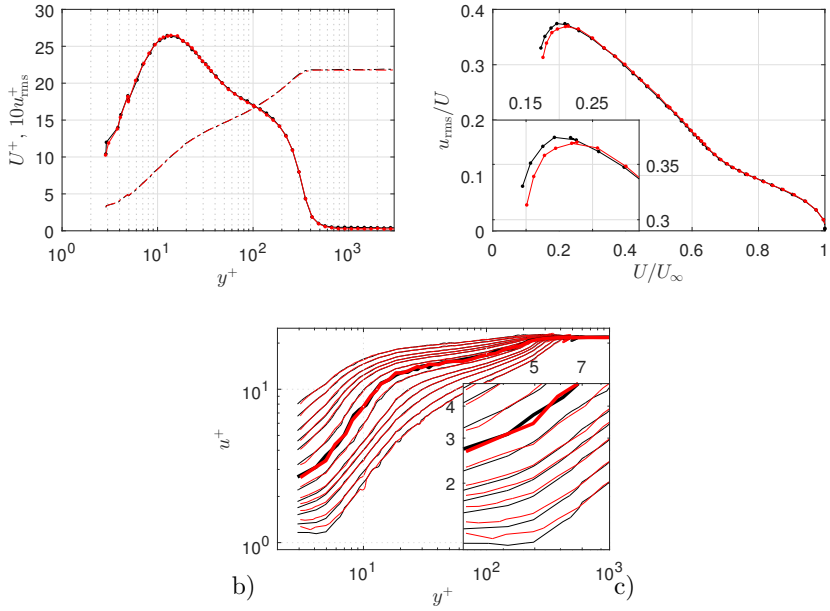

Figure 5: Effect of different resistance overheat ratios a_R in a turbulent boundary layer at $Re_\theta \approx 950$ measured on an aluminum wall: $a_R = 0.3$ (black) and $a_R = 0.8$ (red). a): Inner-scaled mean and rms profile. b): Diagnostic plot with inset highlighting the viscous sublayer. c): Inner-scaled velocity PDF. Thin lines denote 1, 5, 20, 40, 60 and 90 % of the local maximum (thick line) of the PDF.

3.2 Mathematical model

A built-in solver *chtMultiRegionSimpleFoam* capable of calculating conjugate heat transfer in fluid and solid zones is used for the simulation. The governing equations in the fluid region are the conservation of mass, momentum and energy for compressible flow.

$$\frac{\partial\left(\rho^* U_i^*\right)}{\partial x_i^*} = 0 \tag{3}$$

$$\frac{\partial\left(\rho^* U_i^* U_j^*\right)}{\partial x_i^*} = -\frac{\partial P^*}{\partial x_j^*} + \rho^* g_j^* + \frac{1}{\mathrm{Re}}\frac{\partial}{\partial x_i^*}\left[\mu^*\left(\frac{\partial U_j^*}{\partial x_i^*} + \frac{\partial U_i^*}{\partial x_j^*} - \frac{2}{3}\frac{\partial U_k^*}{\partial x_k^*}\delta_{ij}\right)\right] \tag{4}$$

$$\frac{\partial\left(\rho^* h^* U_i^*\right)}{\partial x_i^*} + \frac{\mathrm{Ec}}{2}\frac{\partial\left(\rho^* U_i^* U_j^* U_j^*\right)}{\partial x_i^*} = \frac{1}{\mathrm{RePr}}\frac{\partial}{\partial x_i^*}\left(\frac{k^*}{c_p^*}\frac{\partial h^*}{\partial x_i^*}\right) + \mathrm{Ec}\rho^* U_i^* g_i^* \,. \tag{5}$$

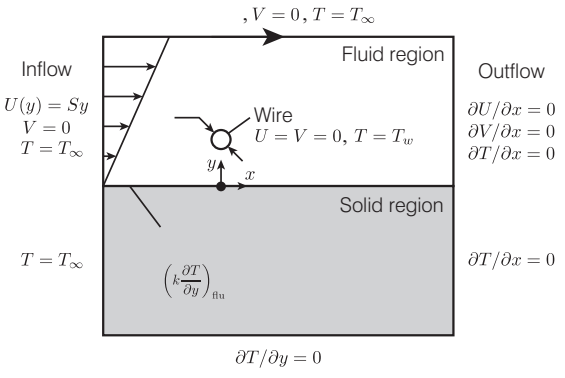

Figure 6: The computational domain with the boundary conditions.

In the solid region, the heat-conduction equation is solved:

$$\frac{k^*}{\rho^* c_p^*}\frac{\partial^2 T^*}{\partial x_i^* \partial x_i^*} = 0.$$

The inlet velocity at the height of the wire centre U_w and the wire diameter d are employed to normalize the velocity components and coordinates, respectively, while the temperature is scaled as $T^* = (T - T_\infty)/(T_w - T_\infty)$. The thermal physical properties ρ^*, μ^*, k^*, and c_p^* (density, dynamic viscosity, thermal conductivity and specific heat at constant pressure, respectively) in the equations are chosen as 7th polynomial functions of temperature and normalized by the corresponding values at inflow temperature T_∞. The other non-dimensional parameters are the Eckert number, the Prandtl number and the Reynolds number, which are defined as follows:

$$\text{Eckert number}: \mathrm{Ec} = \frac{{U_w}^2}{c_{p\infty}\left(T_w - T_\infty\right)}, \tag{6}$$

$$\text{Prandtl number}: \mathrm{Pr} = \frac{\mu_\infty c_{p\infty}}{k_\infty}, \tag{7}$$

$$\text{Reynolds number}: \mathrm{Re} = \frac{\rho_\infty U_w d}{\mu_\infty}. \tag{8}$$

The heat loss from the wire was evaluated as the mean Nusselt number Nu on the wire surface, which is calculated from the local Nusselt number Nu(θ). The heat flux at a certain point on the surface $\dot{q}(\theta)$ is calculated as

$$\dot{q}(\theta) = -k(T_w)\left.\frac{\partial T(r,\theta)}{\partial r}\right|_{r=d/2}, \tag{9}$$

where r and θ are the polar coordinates originated at the wire centre. Normalizing $\dot{q}(\theta)$ with a reference heat flux $\dot{q}_c = k(T_f)(T_w - T_\infty)/d$ to obtain the local Nusselt number:

$$\mathrm{Nu}(\theta) = \frac{\dot{q}(\theta)}{\dot{q}_c} = -\frac{k(T_w)}{k(T_f)}\left.\frac{\partial T^*(r^*,\theta^*)}{\partial r^*}\right|_{r^*=0.5}, \tag{10}$$

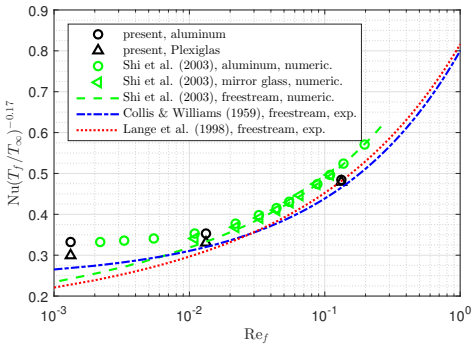

Figure 7: Nusselt number on the wire surface as a function of Reynolds number together with results from previous studies. The result of aluminum/mirror glass wall ($k^* = 29.6$) and the calibration result in a freestream by Shi et al. (2003) are corrected based on their temperature setting of T_∞ and T_w.

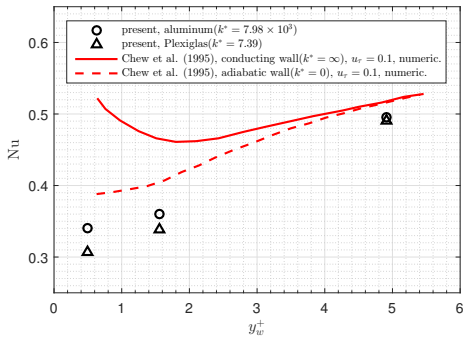

Figure 8: Nusselt number Nu on the wire surface as a function of the inner-scaled height of the wire. The present result is plotted together with that of the previous numerical study employing walls with heat conductivities of $k^* = \infty$ and $k^* = 0$.

where $\theta^* = \theta/(2\pi)$ and T_f is the film temperature: $T_f = (T_w + T_\infty)/2$. By taking the average of Nu over the wire surface, the mean Nusselt number is derived as:

$$\mathrm{Nu} = \int_0^1 \mathrm{Nu}(\theta^*) d\theta^*. \tag{11}$$

3.3 Numerical results

The result of the numerical calculation is plotted in figure 7 in the form

$$\mathrm{Nu}\left(\frac{T_f}{T_\infty}\right)^{-0.17} = f(\mathrm{Re}_f), \tag{12}$$

where the subscript f indicates the corresponding value at the film temperature. This correction of the Nusselt number is proposed by Collis & Williams (1959) to eliminate the effect of the overheat ratio. The results from several previous studies about the heat loss from a hot-wire sensor are also plotted together. The present results shows reasonable agreement in a qualitative tendency with the previous studies and it is again observed that higher conductivity of the material results in larger heat loss.

The Nusselt number as a function of the inner-scaled height of the wire centre y_w^+ is shown in figure 8, where y_w^+ can be calculated as $y_w^+ = y_w\sqrt{S\rho_\infty/\mu_\infty}$. The heat loss difference for the different wall conductivity becomes smaller as y_w^+ increases and almost vanishes when $y_w^+ = 4.9$, which implies that the wall-proximity effect is negligible outside of the viscous sublayer. However, the present result is found to deviate from that of Chew et al. (1995). Apart from the wall conductivity, the difference in the size of computational domain (not mentioned) or the overheat ratio (although the effect of this factor is said to be negligible in their paper) might be the reasons for this discrepancy. Furthermore, the procedure in which they varied the wire height y_w^+ by changing the real-scale position maintaining the velocity gradient S of the inflow is likely to be another reason, which may indicate that not only the inner-scaled height of the wire but also the real-scale distance have an influence on the heat loss.

The field temperature distribution around the wire is shown in figure 9. It is apparent that the heat from the wire hardly remains in the aluminum wall while it does for the Plexiglas wall. For the Plexiglas wall, a high-temperature zone inside the wall shifts further downstream due to the interaction of the temperature wake and the wall as the velocity gradient S increases, i.e. the distance y_w^+ increases. The heat accumulates right beneath the wire for the cases with smaller y_w^+, which causes less heat loss from the wire. However, the Nu for the wire near solid walls are still higher than that of the wire in a freestream far away from a wall.

4 Conclusions

An experimental and numerical investigations of HWA measurement close to solid walls were carried out. Based on the present results, the following conclusions can be drawn:

- The thermal conductivity of the wall material affects the HWA reading, viz., walls with higher thermal conductivity lead to higher output voltages, i.e. larger overestimation of the velocity. It should be noted that highly conductive materials, such as aluminum, brass and steel show similar results despite the fact that the conductivity differs a factor of ten between them, For poorly conductive materials Plexiglas shows a much larger effect than styrofoam, despite the fact that Plexiglas has a thermal conductivity 3 orders of magnitude less than the metals, whereas styrofoam has an order of magnitude further reduced conductivity.
- Employing higher overheat ratios or longer sensors contributes to larger velocity overestimationst as these factors assist the additional heat loss from the sensor.
- The measured turbulence intensity and the velocity PDF are also affected by the wall conductivity and the overheat ratio: employing higher conductivity and higher temperature loading of the wire suppresses the reading of the turbulence intensity, and results in a narrower PDF in the low speed region within the viscous sublayer.
- The difference of the output voltage by varying the parameters can be seen only in the viscous sublayer, and one should note that the effect within the sublayer can easily be "hidden" when measured velocity profiles are employed to determine the absolute wall position and friction velocity as it is common.
- For poorly conducting walls, the heat accumulates beneath the wire inside the wall and it suppresses the additional heat loss. This heat accumulation

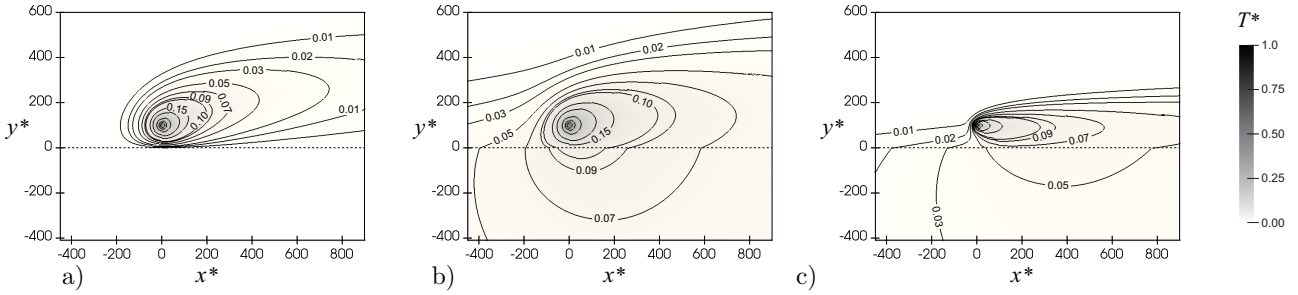

Figure 9: The distribution of temperature T^* around the heated wire above a solid wall. The broken line indicates the interface of the fluid and solid regions. a) Aluminum wall with the velocity gradient of $S = 100\ \mathrm{s}^{-1}$. b) Plexiglas wall with the velocity gradient of $S = 100\ \mathrm{s}^{-1}$. c) Plexiglas wall with the velocity gradient of $S = 1000\ \mathrm{s}^{-1}$.

becomes larger as the inner-scaled height of the wire decreases.

Hence, in order to reduce the wall-effect on hot-wire readings in the viscous sublayer, it is beneficial to perform measurements above low conducting materials as well as operate the hot-wire at a low overheat ratio in order to obtain accurate measurements of both mean and fluctuating velocities.

Acknowledgments

This work was done in the framework of the Keio University-KTH double-degree program and partly supported through JSPS KAKENHI Grant Number JP16K06900.

References

Alfredsson, P. H., Johansson, A. V., Haritonidis, J. H. & Eckelmann, H. (1988), The fluctuating wall-shear stress and the velocity field in the viscous sublayer, *Phys. Fluids*, Vol. 31, pp. 1026-1033.

Alfredsson, P. H. & Örlü, R. (2010), The diagnostic plot–a litmus test for wall bounded turbulence data, *Eur. J. Mech. B-Fluids*, Vol. 29, pp. 403-406.

Alfredsson, P. H., Örlü, R. & Schlatter, P. (2011a) The viscous sublayer revisited–exploiting self-similarity to determine the wall position and friction velocity, *Exp. Fluids*, Vol. 51, pp. 271-280.

Alfredsson, P. H., Segalini, A. & Örlü, R. (2011b), A new scaling for the streamwise turbulence intensity in wall-bounded turbulent flows and what it tells us about the "outer" peak, *Phys. Fluids*, Vol. 23, 041702.

Bhatia, J. C., Durst, F. & Jovanovic, J. (1982), Corrections of hot-wire anemometer measurements near walls, *J. Fluid Mech.*, Vol. 122, pp. 411-431.

Chew, Y., Shi, S. & Khoo, B. (1995), On the numerical near-wall corrections of single hot-wire measurements, *Int. J. Heat Fluid Flow*, Vol. 16, pp. 471-476.

Collis, D. & Williams, M. (1959), Two-dimensional convection from heated wires at low Reynolds numbers, *J. Fluid Mech.*, Vol. 6, pp. 357-384.

Durst, F., Shi, J.M. & Breuer, M. (2002), Numerical prediction of hot-wire corrections near walls, *J. Fluids Eng.*, Vol. 124, pp. 241-250.

Durst, F. & Zanoun, E. S. (2002), Experimental investigation of near-wall effects on hot-wire measurements, *Exp. Fluids*, Vol. 33, pp. 210-218.

George, W. K., Beuther, P. D. & Shabbir, A. (1989), Polynomial calibrations for hot wires in thermally varying flows, *Exp. Therm Fluid Sci.*, Vol. 2, pp. 230-235.

Krishnamoorthy, L., Wood, D., Antonia, R. & Chambers, A. (1985), Effect of wire diameter and overheat ratio near a conducting wall, *Exp. Fluids*, Vol. 3, pp. 121-127.

Lange, C., Durst, F. & Breuer, M. (1998), Momentum and heat transfer from cylinders in laminar crossflow at $10^{-4} \leq \mathrm{Re} \leq 200$, *Int. J. Heat Mass Transfer*, Vol. 41, pp. 3409-3430.

Örlü, R., Fransson, J. H. M. & Alfredsson, P. H. (2010), On near wall measurements of wall bounded flows — The necessity of an accurate determination of the wall position, *Prog. Aerosp. Sci.*, Vol. 46, pp. 353-387.

Örlü, R. Segalini, A., Klewicki J. & P. H. Alfredsson (2016) High-order generalisation of the diagnostic plot to turbulent boundary layers. *J. Turbul.* Vol. 17, pp. 664–677.

Örlü, R. & Schlatter, P. (2011), On the fluctuating wall shear stress in zero pressure-gradient turbulent boundary layer flows, *Phys. Fluids*, Vol. 23, 021704.

Polyakov, A. & Shindin, S. (1978), Peculiarities of hot-wire measurements of mean velocity and temperature in the wall vicinity, *Lett. Heat Mass Transfer*, Vol. 5, pp. 53-58.

Shi, J. M., Breuer, M., Durst, F. & Schäfer, M. (2003), An improved numerical study of the wall effect on hot-wire measurements, *J. Heat Transfer*, Vol. 125, pp. 595-603.

Zanoun, E. S., Durst, F. & Shi, J. M. (2009), The physics of heat transfer from hot wires in the proximity of walls of different materials, *Int. J. Heat Mass Transfer*, Vol. 52, pp. 3693-3705.